Synthesis of electrochromic vanadium oxide by pulsed spray pyrolysis technique and its properties

C E Patil[1], N L Tarwal[3], P S Shinde[3], H P Deshmukh[2] and P S Patil[3,4]

[1] Department of Physics, Bharati Vidyapeeth's MBSK Kanya Mahavidyalay, Kadegaon, Sangli, MS, India

[2] Bharati Vidyapeeth's YM College, Pune, MS, India

[3] Thin Film Materials Laboratory, Department of Physics, Shivaji University, Kolhapur, MS 416 004, India

E-mail: psp_phy@unishivaji.ac.in (P S Patil)

Abstract

A new improved pulsed spray pyrolysis technique (PSPT) was employed to deposit a vanadium oxide (V_2O_5) thin film from a methanolic vanadium chloride precursor onto glass and conducting $F:SnO_2$ coated glass substrates. The structural, morphological, electrical, optical and spectroscopic properties of the film deposited at 573 K were studied. Infrared spectroscopy and x-ray diffraction confirmed the presence of the V_2O_5 phase. The V_2O_5 film (thickness $\sim$118 nm) is polycrystalline with a tetragonal crystal structure. Scanning electron microscopy reveals compact granular morphology consisting of $\sim$80–100 nm size grains. The film is transparent in the visible region (average $\%T \sim$70%) with an optical band gap energy of 2.47 eV involving both direct and indirect optical transitions. The room temperature electrical resistivity (conductivity) of the film is $1.6 \times 10^8 \, \Omega$ cm ($6.25 \times 10^{-9} \, S \, cm^{-1}$) with an activation energy of 0.67 eV in the temperature range 300–550 K. It exhibited cathodic electrochromism in the lithium containing electrolyte (0.5 M $LiClO_4$ + propylene carbonate).

1. Introduction

Vanadium oxide films are receiving increasing interest due to their unique peculiarities such as electrochemical activity, high stability, good specific energy, special layered structure and excellent thermoelectric property. They are widely used in a variety of scientific and technological applications such as active cathode electrodes in rechargeable lithium ion batteries [1–5], electrochromic (EC) devices [6–8], electronic and optical switches [9, 10], catalysis [11] and gas sensing devices [12]. Recently, vanadium oxide nanofibres have been investigated and found to behave like artificial muscles (actuators) that contract reversibly on applying an electrical signal [13]. Vanadium oxide exhibits various phases such as VO, V_2O_3, VO_2, V_4O_9 and V_2O_5, of which VO_2 exhibits metal–insulator transition that occurs over a wide range of transition temperatures depending on the O/V ratio. V_2O_5

is the most stable compound of the V–O system [14]. The stoichiometric V_2O_5 belongs to the $3d^0$ insulators group. Nevertheless, the d^0 insulators are susceptible to loss of oxygen, which gives rise to non-stoichiometric or reduced compounds such as V_2O_{5-x}, causing defects. V_2O_5 thin films have been prepared by various methods such as sputtering [15, 16], vacuum evaporation [17, 18], sol–gel [19, 20], pulsed laser deposition [21], chemical vapour deposition [22], electron-beam evaporation [23], thermal evaporation [24] and spray pyrolysis [25, 26]. However, deposition of thin films by the spray pyrolysis method has grabbed the attention of researchers due to its low-cost set-up and the ability to deposit large area coatings [25]. Nevertheless, very few reports are available on the preparation of V_2O_5 using this method. Bouzidi *et al* [25] synthesized vanadium oxide thin films, for the first time, using the spray pyrolysis technique. Polycrystalline V_2O_5 and V_4O_9 films with orthorhombic structure are obtained using vanadium trichloride (VCl_3) solution (0.1, 0.4 and 0.05 M) at two different substrate temperatures, namely, 473 and

[4] Author to whom any correspondence should be addressed.

523 K. Boudaoud *et al* [26] obtained polycrystalline V_2O_5 thin films by spray pyrolysis at a relatively lower substrate temperature of 423 K using aqueous VCl_3 solution. Akl [27] reported the preparation of V_2O_5 films by spray pyrolysis and investigated the influence of solution molarity on their microstructural, optical and electrical properties. However, such spray deposited V_2O_5 films have been investigated for their use in EC devices.

In this work, we report the synthesis of a polycrystalline V_2O_5 thin film at a substrate temperature of 573 K using a novel pulsed spray pyrolysis technique (PSPT). The PSPT system is different from the conventional spray pyrolysis technique in the sense that it offers great control over the spraying droplets (solution flow rate) and hence on the growth and morphology of the film with the help of electromagnetic solenoids that control the spray ON–OFF time. More importantly, loss of spraying solution is avoided in this way unlike conventional spray pyrolysis techniques. A stable and uniform substrate temperature up to 1073 K can be achieved using the PSPT. Moreover, the films can be grown in ambient atmosphere (inert/oxygen) depending on the requirements. It is possible to grow exotic morphologies using this PSPT [28]. The structural, morphological, electrical, optical and EC properties of V_2O_5 film are investigated.

2. Experimental details

V_2O_5 thin film was deposited by spraying 0.005 M methanolic VCl_3 solution using the PSPT. It is known that pyrolysis of the droplets and subsequent formation of the grain structure, where atoms line up with particular orientation, depend on the droplet resident time (DRT). In the present PSPT system, by varying the ON/OFF timing of the solution solenoid, one can control the DRT and hence the morphology of the film can be altered. This enables controlling the film quality, especially better control over the growth kinetics. An electronic controller is used to control the ON/OFF switching of both the solution and gas electromagnetic solenoids. The solution solenoid pulse time and interval time was adjusted to 9 : 1. Figure 1 shows a schematic of the PSPT; which has been designed, fabricated and patented by us [29]. The precursor solution was sprayed onto the pre-heated glass substrates maintained at a fixed substrate temperature of 573 K. The optimized preparative parameters to obtain a uniform, transparent, pinhole-free thin film are given in table 1. Compressed air at the flow rate of $18\,l\,min^{-1}$ was used as a carrier gas. The spray nozzle-to-substrate distance was optimized at 22 cm. 20 ml of methanolic VCl_3 solution was sprayed. To choose the deposition temperature of V_2O_5, thermogravimetric analysis (TGA) and differential thermal analysis (DTA) of the VCl_3 (99% purity) precursor were carried out using a SDT 2960 (simultaneous DCS-TGA), TA Instruments (USA), to study its thermal decomposition characteristics. The DTA chamber was purged with ambient air. TGA and DTA were performed from 303 to 1073 K at the scan rate of $283\,K\,min^{-1}$ with alumina as a reference material. The powder collected from the deposited film was characterized by infrared (IR) spectroscopy using the Perkin Elmer IR spectrometer model 783 in the spectral range
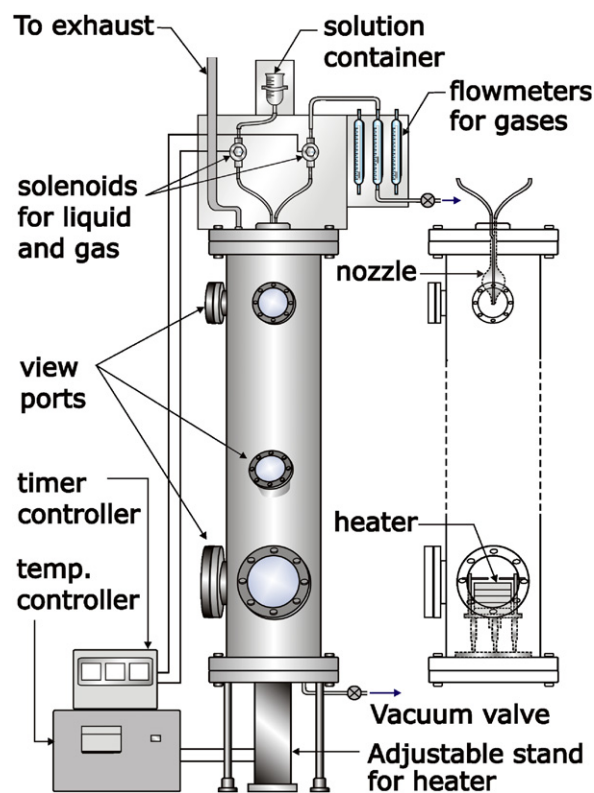
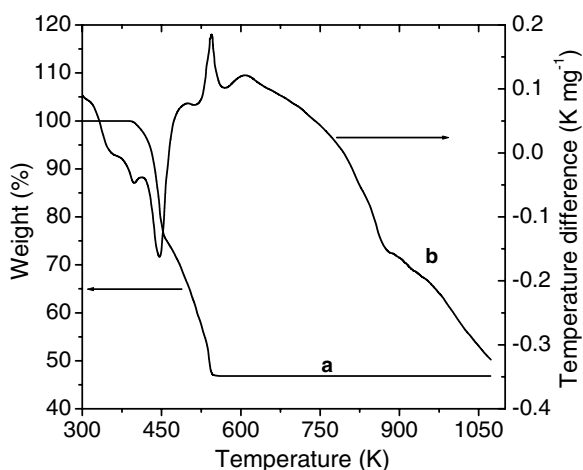

Figure 1. Schematic of the PSPT.

Table 1. Preparative parameters of the V_2O_5 thin film deposited at a substrate temperature of 573 K using the PSPT.

Preparative parameters	Optimized value
Precursor	Vanadium chloride (VCl_3)
Solvent	Methanol
Solution concentration (M)	0.005
Solution quantity (cm^3)	20
Nozzle tip diameter (cm)	0.03
ON : OFF time (s)	9 : 1
Nozzle-to-substrate distance (cm)	22
Air flow rate ($l\,min^{-1}$)	18
Air pressure ($kg\,m^{-2}$)	2.5

450–$4000\,cm^{-1}$. To record IR patterns, the pellet was prepared by mixing KBr with vanadium oxide powder, collected from a thin film, in the ratio 300 : 1 and then pressing the pellet between two pieces of polished steel.

The structural and morphological characterizations were carried out using a Philips-PW 3710 x-ray diffractometer with Cu Kα radiation ($\lambda = 1.5432\,\text{Å}$) and a JEOL JSM-6360 scanning electron microscope (SEM), respectively. The optical study was carried out using a UV–Vis Systronics spectrophotometer in the wavelength range 350–850 nm. A two-probe resistivity unit was used to measure the electrical resistivity of the film in the temperature range 300–550 K.

The EC cell consisted of a conventional three-electrode cell in which a vanadium oxide thin film deposited onto the FTO coated glass substrate ($9\,\Omega/\square$), a graphite plate and a saturated calomel electrode (SCE) served, respectively, as the working electrode, the counter electrode and the reference electrode. $0.5\,M\ LiClO_4$ + propylene

**Figure 2.** (a) TGA and (b) DTA of the precursor powder of vanadium chloride (VCl₃) over 303–1073 K.

Figure 3. The IR spectrum of the as-deposited V_2O_5 thin film deposited at 573 K.

Figure 4. XRD pattern of the as-deposited V_2O_5 thin film at 573 K.

carbonate (PC) was used as the electrolyte solution. The cyclic voltammetry (CV) and chronoamperometry (CA)/chronocoulometry (CC) experiments were carried out using a VersaStat-II (EG and G) potentiostat/galvanostat, controlled by M270 software. All the potentials were referred with respect to SCE.

3. Results and discussion

Figure 2(a) and (b), respectively, show the TGA and DTA thermograms recorded for VCl₃ in the temperature range 303–1073 K at the scan rate of 283 K min⁻¹. The thermal evolution and subsequent weight loss of VCl₃ in air take place in two consecutive stages, for which the inflection points coincide with the temperature corresponding to exothermic and endothermic peaks in the DTA trace. The weight loss of the precursor begins as the precursor gets heated at 303 K. The loss of water from the precursor is attributed to the observed endothermic peaks. The total weight loss corresponding to the removal of both the physisorbed and chemisorbed water is calculated to be about 56.83%. The regular weight loss commences at about 443 K, which is an indication of the onset of thermal decomposition of the precursor. In the temperature range 443–543 K, weight loss is mainly due to the decomposition of vanadium chloride salt, expulsion of Cl ions from the precursor and thermal oxidation of vanadium that leads to the crystallization of vanadium oxide. A broad exothermic hump with a sharp peak affirms these processes. The negligible weight loss beyond 543 K indicates the formation of a stable V_2O_5 phase.

Figure 3 shows the IR spectrum of the powder collected from the V_2O_5 sample in the frequency range 450–4000 cm⁻¹. The spectrum comprises seven absorption peaks: 505.44 cm⁻¹ (ν_1), 719.23 cm⁻¹ (ν_2), 950.18 cm⁻¹ (ν_3), 1123.69 cm⁻¹ (ν_4), 1625.18 cm⁻¹ (ν_5), 2922.84 cm⁻¹ (ν_6) and 3390.70 cm⁻¹ (ν_7). It is in consensus that the peaks in the range from 1025 to 900 cm⁻¹ are attributed to the stretching vibration of unshared V=O bonds. Culea *et al* [30] observed IR absorption bands at 825 and 1020 cm⁻¹ for crystalline V_2O_5. The bands obtained at 950.18, 719.23, 505.44 cm⁻¹
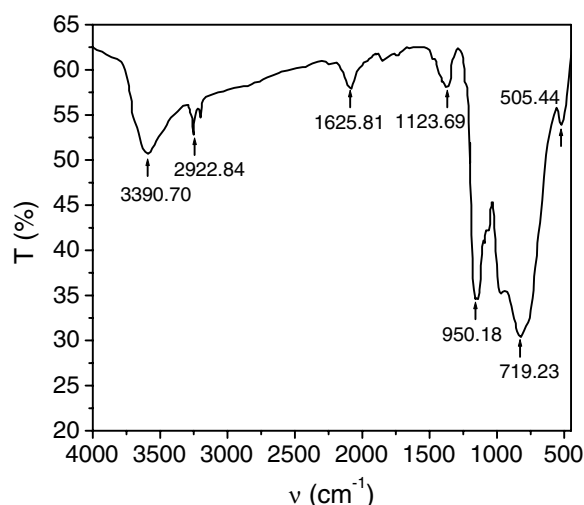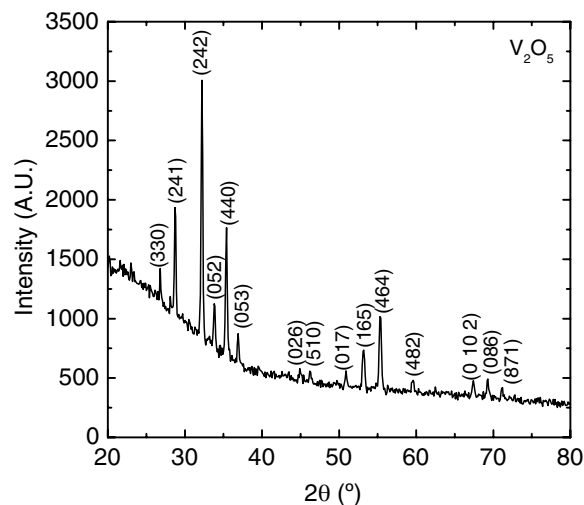
are similar to those obtained by Ivanova *et al* [31] and Benmouss *et al* [32] for polycrystalline V_2O_5. The existence of ν_1 has also been found by others at about 525 cm⁻¹, 535 cm⁻¹ and has been attributed to the stretching mode of the oxygen atoms, which are shared between three vanadium atoms [33]. The water bending vibrations have produced ν_5, ν_6 and ν_7 bands. The inclusion of water molecules might be due to the retention of water of crystallization in the sample at the deposition temperature of 573 K and the absorption of water during mixing and pelleting with KBr. This result affirms the formation of the hydrated V_2O_5 phase deposited at 573 K.

The V_2O_5 phase formation is further confirmed by the x-ray diffraction study. Figure 4 shows the x-ray diffraction (XRD) pattern of the V_2O_5 thin film prepared at 573 K in the diffracting angle (2θ) range of 20°–80°. The observed XRD pattern is compared with the standard diffraction data (lattice parameters: $a = 14.259$ Å, $b = 14.259$ Å and $c = 12.576$ Å) [34]. Well-resolved peaks characterizing the tetragonal crystal structure are observed in the XRD pattern of the V_2O_5 film. Besides the major peak of (2 4 2), planes along (3 3 0), (2 4 1),
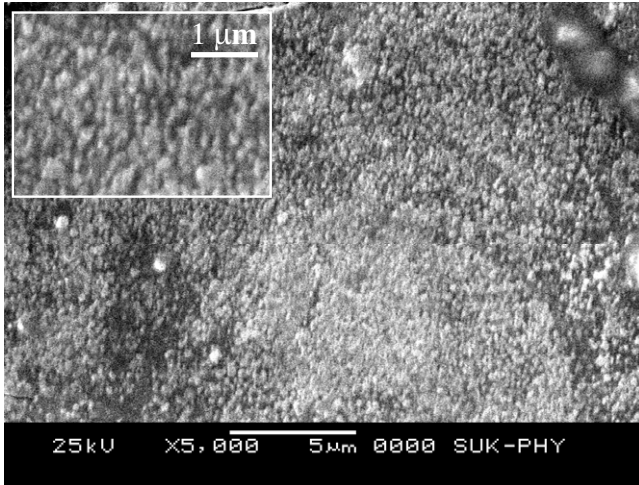
Figure 5. Typical SEM image of the V_2O_5 thin film deposited at 573 K. The inset shows the SEM image of the same film at $\times 10\,000$ magnification.

(0 5 2), (4 4 0), (0 5 3), (0 2 6), (5 1 0), (0 1 7), (1 6 5), (4 6 4), (4 8 2), (0 10 2), (0 8 6) and (8 7 1) are also observed. The lattice parameters were calculated using relation (1):

$$\frac{1}{d^2} = \frac{(h^2 + k^2)}{a^2} + \frac{l^2}{c^2}. \tag{1}$$

The values of the lattice parameters $a = b = 14.3\,\text{Å}$ and $c = 12.4\,\text{Å}$ are comparable to those of V_2O_5 [34].

　　Figure 5 shows an SEM image of the V_2O_5 thin film deposited at 573 K, recorded with $\times 5000$ magnification. The inset shows the SEM image at $\times 10\,000$ magnification. The SEM image reveals the compact granular morphology of V_2O_5 devoid of any cracks having grains of size 80–100 nm.

　　The optical absorption and transmission spectrum for the V_2O_5 thin film is recorded in the wavelength range of 350–850 nm at room temperature. The optical absorption coefficient of the film can be evaluated from transmittance (2) [35] as

$$T = A \exp(-\alpha t), \tag{2}$$

where T is the transmittance, t is the film thickness, A is the coefficient related to the refractive index, which is nearly equal to unity at the absorption edges, and α is the absorption coefficient. The value of absorption coefficient is of the order of $10^4\,\text{cm}^{-1}$. The absorption coefficient is given by the following relation (3) [36],

$$\alpha = \frac{\alpha_0 (h\nu - Eg)^n}{h\nu}, \tag{3}$$

where $h\nu$ is the incident photon energy, α_0 the edge width parameter and n an exponent that determines the type of electronic transition causing absorption, which is 1/2, 3/2, 2 and 3 for direct allowed, direct forbidden, indirect allowed and indirect forbidden transition, respectively. The exponential dependence of absorption on the incident photon energy near the fundamental absorption edge may be due to the electronic transitions involved in the localized states formed in the band gap. The oxygen vacancies are formed in oxygen layers when V_2O_5 films are formed at elevated temperatures. Empty 3d
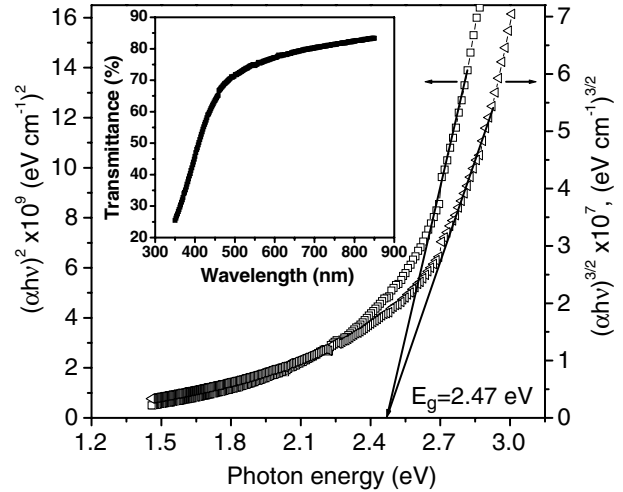
Figure 6. Plot of $(\alpha h\nu)^2$ versus photon energy of the as-deposited V_2O_5 thin film deposited on glass substrate at 573 K. The inset shows the transmittance spectra of the as-deposited V_2O_5 thin film deposited on glass at 573 K.
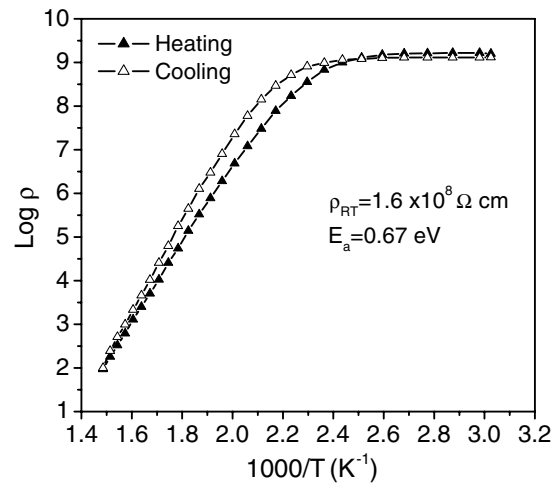
Figure 7. An Arrhenius plot (log ρ versus $1000/T$) of the V_2O_5 thin film deposited at 573 K.

orbitals of vanadium atoms adjacent to a vacancy are able to localize excess electrons. This leads to the formation of localized states. This phenomenon was also observed by others for V_2O_5 in bulk and thin film forms [37]. The optical absorption coefficient, α, determined from the experimental transmittance and absorbance data for the V_2O_5 film is found to give a better fit when $n = 1/2$ and 3 in relation (3) suggesting, respectively, the direct allowed and indirect forbidden transitions. Figure 6 shows the variation of $(\alpha h\nu)^2$ and $(\alpha h\nu)^{3/2}$ versus photon energy ($h\nu$), respectively, for direct allowed and indirect forbidden optical transitions. The band gap energy (E_g) of the film is obtained by extrapolating the linear region of the plot to zero absorption coefficient (i.e. at $\alpha = 0$). The estimated value of E_g for the V_2O_5 film is 2.47 eV, which is in agreement with the reported values for V_2O_5 [25, 26]. The film exhibits 70% average optical transmittance in the visible region as seen in the inset of figure 6.

　　Figure 7 shows the Arrhenius plot exhibiting inverse temperature dependence of the resistivity for the as-deposited

V_2O_5 film during heating and cooling, thereby supporting the semiconducting nature of V_2O_5. The resistivity of V_2O_5 is determined using relation (4),

$$\rho = \frac{\pi}{\ln 2}\left(\frac{V}{I}\right)t, \tag{4}$$

where V is the applied voltage, I is the current and t is the thickness of the film. Here, the correction factor is assumed to be unity. The room temperature electrical resistivity (ρ_{RT}) was of the order of $10^8\,\Omega\,cm$.

V_2O_5 is generally a non-stoichiometric compound because of oxygen vacancies, compensated by excess electrons located on vanadium sites, reducing V^{5+} to V^{4+} and contributing to the electronic conductivity. V_2O_5 is known as a typical low-mobility n-type semiconductor [38]. The electric transport mechanism in vanadium-based materials is generally governed by the presence of vanadium in various valency states and it is well established that these are electronic conductors in which the conduction is due to the exchange of electrons between V^{4+} and V^{5+} ions [39]. The dc conductivity of monocrystalline V_2O_5 is found to be anisotropic owing to the structure: it is larger along the *b*-axis and smaller along the *c*-axis ($\sigma_b \gg \sigma_a \gg \sigma_c$). ESR and dc conductivity studies [40–42] of the non-stoichiometric V_2O_5 single crystal suggest the presence of free and bound small polarons. In this way, the unpaired electron gets localized on two vanadium sites associated with an oxygen vacancy leading to the formation of a 'bound polaron'. Austin *et al* and Murawski *et al* studied the non-stoichiometric character of amorphous V_2O_5. The V^{4+} ions are produced as a consequence of the formation of oxygen vacancies. Due to the highly polar character of the network, small polarons are formed around V^{4+} ions. Electrical transport has been reported to arise from the thermally activated electronic hopping between V^{4+} and V^{5+} ions [43, 44]. Abo El Soud *et al* [45] showed that conduction in V_2O_5 occurs via a complex charge transfer mechanism. The conductivity is dependent on the concentration of V^{4+} ions as well as on the average separation distance between vanadium ions. Coustier *et al* and Muster *et al* also showed that electronic conductivity of a dense V_2O_5 xerogel network proceeds by hopping between V^{5+} and V^{4+} sites [46, 47].

The film shows linear behaviour (in figure 7) over the temperature range 300–420 K following Mott's small polaron hopping (SPH) model [42, 48] based on the single optical phonon approach and is independent of temperature after 420 K. The SPH model predicts the resistivity in non-adiabatic approximation as [42]

$$\rho = \rho_o \exp\left(\frac{E_a}{kT}\right), \tag{5}$$

where ρ_o is the pre-exponential factor, k Boltzmann's constant and T the absolute temperature. The activation energy (E_a) is calculated using relation (5) and the slope of graph ($\log \rho$ versus T^{-1}). The calculated value of activation energy is 0.67 eV. Ramana *et al* [49] reported an activation energy of 0.42 eV, for V_2O_5 thin films prepared by electron-beam evaporation, in the temperature range 303–523 K. The
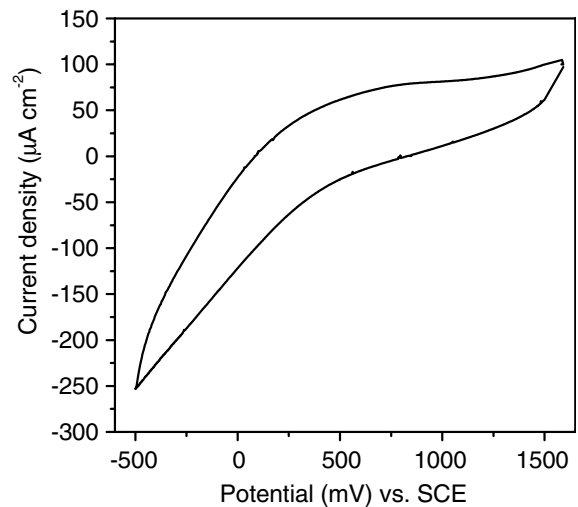
Figure 8. Cyclic voltammogram of the V_2O_5 thin film recorded at the scan rate of $20\,mV\,s^{-1}$.

activation energy in amorphous V_2O_5 thin films appears to be much larger ($\sim$0.7 eV) owing to the more disordered state of the amorphous layer deposited from the vapour state [50–52]. The activation energy of 0.67 eV observed in this study could be due to the higher resistivity of the film owing to a more disordered state of lattice.

The aim of this study is to test the EC performance of the PSPT grown V_2O_5 thin film. Figure 8 shows the CV spectrum recorded for the V_2O_5 film over +1.5 to -0.5 V (versus SCE) at the potential sweep rate of $20\,mV\,s^{-1}$ in the (0.5 M $LiClO_4$ + PC) electrolyte. During the cathodic scan simultaneous intercalation of electrons and Li^+ ions into the V_2O_5 matrix causes progressive reduction in pentavalent vanadium (V^{5+}) to its lower valance state (V^{4+}), thereby forming a coloured vanadium bronze ($Li_xV_2O_5$) according to the well-known mechanism [53]

$$V_2O_5 + xLi^+ + xe \longleftrightarrow Li_xV_2O_5.$$
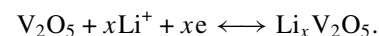
The diffusion coefficient of Li^+ ions is calculated from the Randell–Sevcik equation (6),

$$i_p = 2.72 \times 10^5 n^{3/2} A D^{1/2} C_0 \nu^{1/2}, \tag{6}$$

where D is the diffusion coefficient ($cm^2\,s^{-1}$), C_0 the concentration of active ions in the solution (mol cm^{-3}), ν the scan rate (V s^{-1}), n the number of electrons transferred/molecule, A the electrode area (cm^2) and i_p the peak current density (i_{pa} anodic and i_{pc} cathodic, A). The diffusion constant (D) of $1.37 \times 10^{-8}\,cm^2\,s^{-1}$ is estimated at $20\,mV\,s^{-1}$. The diffusion coefficient of Li^+ ions into solid vanadium oxide is an important factor. The diffusion coefficient has been calculated by various techniques and found to be in good agreement with others [54].

The analysis of CA data is based on the Cottrell equation, which defines the current–time (i–t) dependence for linear diffusion control:

$$i = nFAC_0D^{1/2}\pi^{-1/2}t^{-1/2}, \tag{7}$$

J. Phys. D: Appl. Phys. **42** (2009) 025404

C E Patil *et al*
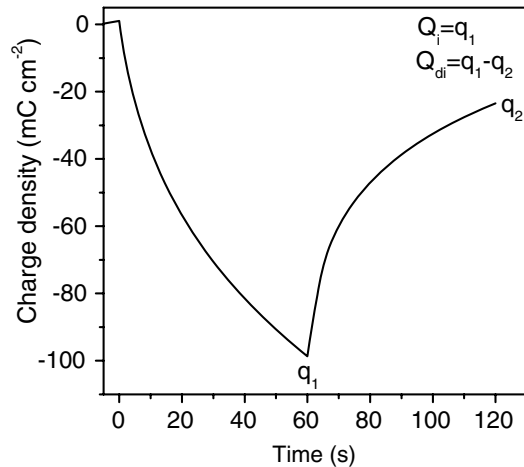
Figure 9. CC curve for the V_2O_5 thin film at a potential step of ± 0.5 V versus SCE.

Figure 10. An optical transmittance spectra of the coloured and bleached samples.

where F is Faraday's constant ($96\,500$ C mol^{-1}) and A is the electrode area (cm^2).

CC involves the measurement of the charge versus time response to an applied potential step waveform. The equation for the Q versus t curve (the Anson equation) is obtained by integrating the Cottrell equation as

$$Q = 2nFAC_0 D^{1/2} \pi^{-1/2} t^{1/2}. \tag{8}$$

The response time for coloration and bleaching is calculated from CA studies (i.e. current transient data). The bleaching kinetics is always faster than the colouring rate for the V_2O_5 film owing to the well-defined mechanisms controlling the two processes. The bleaching speed is governed by the space charge limited current flow of cations through the bulk of the film whereas in the colouring mode the potential barrier at the V_2O_5–electrolyte interface and the number of Li$^+$ ions intercalated play a critical role.

The number of Li$^+$ ions intercalated and deintercalated with respect to time is determined using CC studies, which can be further used to estimate reversibility and coloration efficiency (CE).

Figure 9 shows the CC plot of the V_2O_5 film at a potential step of ± 0.5 V versus SCE for coloured and bleached states for 60 s. The reversibility of the film was determined to be about 77%. The low value of reversibility could be directly attributed to the microstructure of the film, the compact morphology of which does not allow easy passage for the charge carriers to traverse.

Figure 10 shows the optical transmittance spectra of the V_2O_5 film in its coloured and bleached states in the wavelength range 350–1000 nm. The CE at $\lambda = 630$ nm is determined using relation (9),

$$\text{CE}_{(\lambda=630\,\text{nm})} = \frac{\Delta\text{OD}}{Q_i} = \frac{\ln[T_b/T_c]_{\lambda=630\,\text{nm}}}{q/A}, \tag{9}$$

where ΔOD is the change in optical transmittance at a wavelength of 630 nm, Q_i is the amount of charge intercalated into the sample, which was estimated by integrating the area under the curve of current density versus time and T_b and T_c are
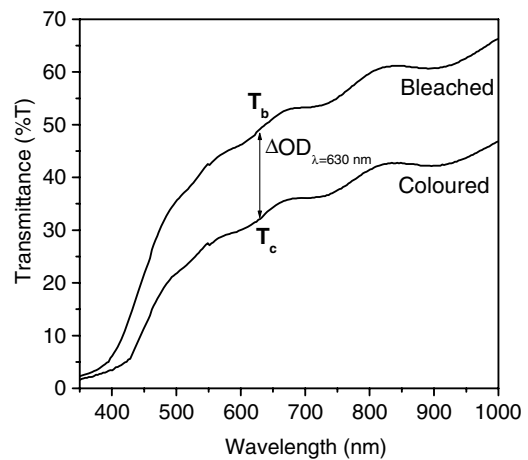
the transmittance values of the bleached state and the coloured state of the V_2O_5 film, respectively. The CE determined at $\lambda = 630$ nm is found to be 13 cm^2 C^{-1}, which is in agreement with the reported values [55]. The electrochemical stability of the film is one of the important parameters to be taken into account when one looks for its applications. Therefore, the film is further tested for long time electrochemical cycling and found to be stable for about 10^4 colour/bleach (c/b) cycles. Hence, such V_2O_5 thin films can be used in conjunction with EC tungsten oxide films for charge-balanced devices for display purposes in informatics, variable reflectance mirrors, smart windows and surfaces with tunable emittance for temperature control of space vehicles.

4. Conclusions

A polycrystalline V_2O_5 sample (film thickness $\sim$118 nm) with a tetragonal crystal structure is prepared from a methanolic vanadium chloride precursor at a substrate temperature of 573 K using a novel PSPT. V_2O_5 is transparent (average optical transmittance $\sim$70%) with a band gap energy of 2.47 eV, involving both direct and indirect optical transitions. The SEM reveals compact granular morphology of V_2O_5 having grains of size $\sim$80–100 nm. V_2O_5 obeyed a non-adiabatic SPH conduction mechanism due to electronic hopping from a lower valence state V^{4+} to a higher valence state V^{5+}. The room temperature electrical resistivity of the film is 1.6×10^8 Ω cm with an activation energy of 0.67 eV. The CE and diffusion constant for the V_2O_5 thin film are found to be 13 cm^2 C^{-1} and 1.37×10^{-8} cm^2 s^{-1}, respectively. It exhibited cathodic electrochromism in the (0.5 M LiClO$_4$ + propylene carbonate) electrolyte.

to Bharati Vidyapeeth University, Pune, and S R Barman, Inter University Consortium for DAE Facilities (IUC-DAEF), Indore, India.

References

[1] Bates J B, Gruzalski G R, Dudney N J, Luck C F, Yu X-H and Jones S D 1993 *Solid State Technol.* **36** 59
[2] Li Y M and Kudo T 1996 *Solid State Ion.* **86/88** 1295
[3] Koike S, Fujieda T, Sakai T and Higuchi S 1999 *J. Power Sources* **81–82** 581
[4] Polo Da Fonseca C N, Davalos J, Kleinke M, Fantini M C A and Gorenstein A 1999 *J. Power Sources* **81–82** 575
[5] Li Y-M, Hibino M, Tanaka Y, Wada Y, Noguchi Y, Takano S and Kudo T 2001 *Solid State Ion.* **143** 67
[6] Cogan S F, Nguyen N M, Perrotti S T and Rauph R D 1988 *Proc. Soc. Photo—Opt. Instrum. Eng.* **57–62** 1016
[7] Rauh R D and Cogan S F 1988 *Solid State Ion.* **28/29** 1707
[8] Anderson A M, Granqvist C G and Stevens J R 1989 *Appl. Opt.* **28** 3295
[9] Nadkarni G S and Shirodkar V S 1983 *Thin Solid Films* **105** 115
[10] Hirashima H, Ide M and Yoshida T 1986 *J. Non-Cryst. Solids* **86** 327
[11] Sawunyama P, Yasumori A and Okada K 1998 *Mater. Res. Bull.* **33** 705
[12] Capone S, Rella R, Siciliano P and Vasanelli L 1999 *Thin Solid Films* **350** 264
[13] Gu G, Schmid M, Chiu P-W, Minett A, Fraysse J, Kim G-T, Roth S, Kozlov M, Muñoz E and Baughman R H 2003 *Nature Mater.* **2** 316
[14] Chatterjee P, Sen Gupta S P and Suchitra S 2001 *Bull. Mater. Sci.* **24** 173
[15] Ottaviano L, Pennisi A, Simone F and Salvi A M 2004 *Opt. Mater.* **27** 307
[16] Krishna M G, Debauge Y and Bhattacharya A K 1998 *Thin Solid Films* **312** 116
[17] Wu G, Du K, Xia C, Kun X, Shen J, Zhou B and Wang J 2005 *Thin Solid Films* **485** 284
[18] RajendraKumar R T, Karunagaran B, SenthilKumar V, Jeyachandran Y L, Mangalaraj D and Narayandass Sa K 2003 *Mater. Sci. Semicond. Proc.* **6** 543
[19] Shtmizu Y, Nagase K, Miura N and Yamazoe N 1992 *Solid State Ion.* **53–56** 490
[20] Viver V, Farcy J and Pereira-Ramos J-P 1998 *Electrochim. Acta* **44** 831
[21] Julien C, Haro-Poniatowski E, Camacho-Lopez M A, Escobar-Alarcon L and Jimenez-Jarquin J 1999 *Mater. Sci. Eng. B* **65** 170
[22] Thi B N B, Minh T P and Simona B 1996 *J. Appl. Phys.* **80** 7041
[23] Rmana C V, Hussain O M and Srinivasulu Naidu B 1997 *Mater. Chem. Phys.* **50** 195
[24] Cheng K-C, Chen F-R and Kai J-J 2006 *Sol. Energy Mater. Sol. Cells* **90** 1156

[25] Bouzidi A, Benramdane N, Nakrela A, Mathieu C, Khelifa B, Desfeux R and Da Costa A 2002 *Mater. Sci. Eng. B* **95** 141
[26] Boudaoud L, Benramdane N, Desfeux R, Khelifa B and Mathieu C 2006 *Catal. Today* **113** 230
[27] Akl A A 2006 *Appl. Surf. Sci.* **252** 8745
[28] Bathe S R and Patil P S 2008 *Solid State Ion.* **179** 314
[29] Patil P S and Sadale S B 2008 An improved spray pyrolysis process for the preparation of good quality thin film semiconducting coatings and apparatus therefore *Indian Patent No* 214163
[30] Culea E, Nicula A L and Bratu I 1984 *Phys. Status Solidi* **83** k15
[31] Ivanova T, Harizanova A and Surtchev M 2002 *Mater. Lett.* **55** 327
[32] Benmoussa M, Ibnouelghazi E, Bennouna A and Ameziane E L 1995 *Thin Solid Films* **265** 22
[33] Abello L, Husson E, Repelin Y and Lucazeau G 1983 *Spectrochim. Acta A* **39** 641
[34] Powder Diffraction File Alphabetic PDF-2 Database, International Center of Diffraction Data, Newtown Square, PA, USA, 2004, File Nos 00-045-1074 and 01-089-2482
[35] Tang X G, Zhou Q F and Zhang J X 2000 *Thin Solid Films* **375** 159
[36] Shinde P S, Patil P S, Bhosale P N and Bhosale C H 2008 *J. Am. Ceram. Soc.* **91** 1266
[37] Kenny N, Kannewurf C R and Whitmore D H 1966 *J. Phys. Chem. Solids* **27** 1237
[38] Patrina I B and Ioffe V A 1965 *Sov. Phys.—Solid State* **6** 2581
[39] Sayer M and Mansingh A 1983 *J. Non-Cryst. Solids* **58** 91
[40] Ioffe V A and Patrina I B 1970 *Phys. Status Solidi* **40** 389
[41] Sanchez C, Henry M, Morineau R and Leroy M C 1984 *Phys. Status Solidi* **22** 175
[42] Sanchez C, Henry M, Grenet J C and Livage J 1982 *J. Phys. C: Solid State Phys.* **15** 7133
[43] Austin I G and Mott N F 1969 *Adv. Phys.* **18** 41
[44] Murawski D, Chung C H and Mackenzie J D 1979 *J. Non-Cryst. Solids* **32** 91
[45] Abo El Soud A M, Mansour B and Soliman L I 1994 *Thin Solid Films* **247** 140
[46] Coustier F, Passerini S and Smyrl W H 1998 *J. Electrochem. Soc.* **145** L73
[47] Muster J, Kim G T, Krstiæ V, Park J G, Park Y W, Roth S and Burghard M 2000 *Adv. Mater.* **12** 420
[48] Mott N F 1968 *J. Non-Cryst. Solids* **1** 1
[49] Ramana C V, Hussain O M, Naidu B S, Julien C and Balkanski M 1998 *Mater. Sci. Eng. B* **52** 32
[50] Koffyberg F P and Benko F A 1978 *Phil. Mag. B* **38** 357
[51] Allersma T, Hakim R, Kennedy T N and Mackenzie J D 1967 *J. Chem. Phys.* **46** 154
[52] Sanchez C, Morineau R and Livage J 1983 *Phys. Status Solidi a* **76** 661
[53] George J and Radhakrishnan M M 1980 *Solid State Commun.* **33** 987
[54] Andrukaitis E and Hill I 2004 *J. Power Sources* **136** 290
[55] Granqvist C G 1995 *Handbook of Inorganic Electrochromic Materials* (Amsterdam: Elsevier) p 331